Article:
Stubbendorff, Christine, Hale, Ed, Bast, Tobias et al. (5 more authors) (2023) Dopamine D1-like receptors modulate synchronized oscillations in the hippocampal-prefrontal-amygdala circuit in contextual fear. Scientific reports. 17631. ISSN 2045-2322

https://doi.org/10.1038/s41598-023-44772-6

scientific reports

Check for updates

OPEN

Dopamine D1-like receptors modulate synchronized oscillations in the hippocampal–prefrontal–amygdala circuit in contextual fear

Christine Stubbendorff[1,6]✉, Ed Hale[1,7], Tobias Bast[2,3], Helen J. Cassaday[2,3], Stephen J. Martin[4], Sopapun Suwansawang[5,8], David M. Halliday[5] & Carl W. Stevenson[1,3]✉

Contextual fear conditioning (CFC) is mediated by a neural circuit that includes the hippocampus, prefrontal cortex, and amygdala, but the neurophysiological mechanisms underlying the regulation of CFC by neuromodulators remain unclear. Dopamine D1-like receptors (D1Rs) in this circuit regulate CFC and local synaptic plasticity, which is facilitated by synchronized oscillations between these areas. In rats, we determined the effects of systemic D1R blockade on CFC and oscillatory synchrony between dorsal hippocampus (DH), prelimbic (PL) cortex, basolateral amygdala (BLA), and ventral hippocampus (VH), which sends hippocampal projections to PL and BLA. D1R blockade altered DH–VH and reduced VH–PL and VH–BLA synchrony during CFC, as inferred from theta and gamma coherence and theta-gamma coupling. D1R blockade also impaired CFC, as indicated by decreased freezing at retrieval, which was characterized by altered DH–VH and reduced VH–PL, VH–BLA, and PL–BLA synchrony. This reduction in VH–PL–BLA synchrony was not fully accounted for by non-specific locomotor effects, as revealed by comparing between epochs of movement and freezing in the controls. These results suggest that D1Rs regulate CFC by modulating synchronized oscillations within the hippocampus–prefrontal–amygdala circuit. They also add to growing evidence indicating that this circuit synchrony at retrieval reflects a neural signature of learned fear.

Learning that certain environments predict threat is adaptive and can be investigated using contextual fear conditioning (CFC) in rodents. During CFC, unsignalled presentation of an aversive unconditioned stimulus (US; e.g. footshock) typically occurs in a novel context. This results in the encoding of a representation of the context, which becomes associated with the US. Fear-related behavior (e.g. freezing) is then elicited in the conditioned context during later memory retrieval[1]. CFC provides a useful model for studying the neurobiological mechanisms underpinning emotional learning, which is also translationally relevant since aberrant emotional memory processing is a key feature of various anxiety-related disorders[2,3].

CFC requires coordinated activity within a distributed neural network that includes the hippocampus, amygdala, and prefrontal cortex (PFC). The context representation is thought to be encoded in dorsal hippocampus (DH) and conveyed to basolateral amygdala (BLA) for association with the US representation[1,2,4,5]. Other evidence indicates that DH is also involved in forming and storing the context-US association[3,6]. Prelimbic (PL) PFC plays a role in processing the context and US representations through its inter-connections with DH and

[1]School of Biosciences, University of Nottingham, Sutton Bonington Campus, Loughborough LE12 5RD, UK. [2]School of Psychology, University of Nottingham, University Park, Nottingham, UK. [3]Neuroscience@Nottingham, University of Nottingham, Nottingham, UK. [4]Cellular and Systems Medicine, Ninewells Hospital and Medical School, University of Dundee, Dundee, UK. [5]School of Physics, Engineering and Technology, York Biomedical Research Institute, University of York, Heslington, York, UK. [6]Present address: Department of Neuroscience and Brain Technologies, Istituto Italiano di Tecnologia, Via Morego 30, 16163 Genova, Italy. [7]Present address: Envigo, Hillcrest, Dodgeford Lane, Belton LE12 9TE, UK. [8]Present address: Faculty of Science and Technology, Nakhon Pathom Rajabhat University, Nakhon Pathom, Thailand. ✉email: christine.stubbendorff@iit.it; carl.stevenson@nottingham.ac.uk

BLA[7–9]. Importantly, DH projects to BLA and PL indirectly through ventral hippocampus (VH), which is also involved in encoding representations of the context and US via its inter-connections with BLA and PL[10–16].

In contrast to the neural circuit basis of CFC, its regulation by neuromodulators remains unclear[17]. Dopamine regulates CFC via D1-like receptor (D1R) signalling in the hippocampal-prefrontal–amygdala circuit[18]. These brain areas receive midbrain dopamine projections and express D1Rs[19–21]. D1R signalling modulates activity in these areas by tuning the balance between excitatory and inhibitory inputs. D1R modulation of this excitability therefore exerts a strong influence on local activity and functional interactions in this circuit[18]. Systemic D1R blockade impairs the acquisition of contextual fear[22–24]. In terms of the brain areas involved, blocking D1Rs locally in DH, PL, or BLA, but not VH, disrupts CFC[23,24]. D1R blockade also interferes with in vitro and in vivo long-term potentiation (LTP), a model of synaptic plasticity that underpins learning, in these areas[25–27]. While it is hypothesized that D1Rs regulate CFC by modulating synaptic plasticity in this circuit[18], the neurophysiological mechanisms linking D1R modulation of LTP and CFC remain unclear.

Synaptic plasticity underpinning learning is facilitated by synchronized rhythmic oscillations that mediate communication between inter-connected brain areas. Theta and gamma synchrony and phase-amplitude coupling (PAC) in the hippocampal–prefrontal–amygdala circuit are important for learned fear processing[28–33]. Interestingly, D1Rs modulate oscillatory activity in and synchrony between these areas[34–41], raising the possibility that D1R blockade impairs LTP and CFC by disrupting synchronized oscillations in this circuit. In this study we examined the effects of systemic D1R blockade on theta and gamma oscillations in DH, VH, PL, and BLA during CFC. Since synchronized oscillations and PAC in this circuit play a role in fear memory retrieval[28–32,42–44], we also examined the effects of impaired CFC by D1R blockade on oscillatory synchrony between these areas at retrieval.

Results

D1R blockade impairs CFC

To determine if D1Rs regulate CFC, we examined the effects of the selective D1R antagonist SCH23390 given systemically (0.1 mg/kg, i.p.) before CFC on freezing at retrieval (Fig. 1A–C). SCH23390 (n = 20) impaired CFC, as indicated by reduced freezing during retrieval testing, compared to vehicle-treated controls (n = 22). For freezing throughout the test session (Fig. 1B), an unpaired t-test revealed that SCH23390 resulted in decreased freezing, compared to vehicle ($t_{(40)} = 2.65$, $P = 0.012$). This was confirmed by the time course analysis (Fig. 1C), which showed that SCH23390 resulted in decreased freezing throughout retrieval, compared to vehicle. Two-way ANOVA revealed a significant main effect of treatment ($F_{(1,40)} = 7.01$, $P = 0.012$) but no main effect of time ($F_{(4,160)} = 2.32$, $P = 0.059$) or treatment × time interaction ($F_{(4,160)} = 0.74$, $P = 0.57$). This confirms previous results showing that SCH23390 impairs CFC[22–24].

Acute D1R blockade alters intra-hippocampal and reduces hippocampal-prefrontal and hippocampal-amygdala synchrony during conditioning

Examples of electrode placements in and local field potentials (LFPs) recorded from each area before US presentations during CFC are shown in Fig. 1D. Schematic representations of theta (4–12 Hz), low gamma (30–45 Hz), and high gamma (55–80 Hz) oscillations, and theta-gamma PAC, are shown in Fig. 1E. Compared to the behavioral data analysis, fewer rats were included in the electrophysiological data analyses because of missed electrode placements or electrical noise artefacts contained in the data. For the analyses comparing between epochs of movement and freezing at retrieval in vehicle-treated controls, the numbers of controls included in these comparisons were unequal because some animals had no movement or freezing epochs based on the criteria defined for their inclusion in the analyses (see Methods). The numbers of animals included in the final datasets for each comparison (SCH23390 vs. vehicle treatment; movement vs freezing in vehicle-treated controls) are indicated in Figs. 2, 3, 4, 5, 6, and 7.

To determine if D1Rs modulate theta oscillations in the hippocampus–prefrontal–amygdala circuit during the conditioning session, we examined the acute effects of SCH23390 on theta power in each area in the 2 min period before US presentations during CFC (Fig. 2A). Differences between SCH23390 and vehicle treatment in power at each individual frequency throughout the theta band were quantified using a log ratio test. In vehicle-treated controls there was a prominent peak ~ 7–8 Hz in hippocampus, whereas this peak was less pronounced in PL and BLA. In DH, SCH23390 decreased peak theta power (7–9 Hz) and increased power outside the peak (4–6 and 11–12 Hz), compared to vehicle ($P < 0.001$). The largest effect of SCH23390 on theta power was observed in VH, where it reduced peak power (7–9 Hz) while also increasing power at higher frequencies (11–12 Hz), compared to vehicle ($P < 0.001$). SCH23390 had no effect on theta power in PL or BLA.

To determine if D1Rs modulate theta synchrony before CFC, we examined the acute effects of SCH23390 on theta coherence in this circuit (Fig. 2B). Differences between SCH23390 and vehicle treatment in coherence between the areas sharing direct anatomical connections (i.e. DH–VH, VH–PL, VH–BLA, and PL–BLA) were quantified at each individual frequency throughout the theta band using a chi-squared difference of coherence test. Vehicle-treated controls showed peaks for theta coherence ~ 7–9 Hz. SCH23390 decreased peak theta coherence between DH and VH (7–8 Hz), while increasing coherence outside the peak (4–6 and 11–12 Hz), compared to vehicle ($P < 0.001$). The largest effects of SCH23390 were observed on VH–PL and VH–BLA theta coherence, where SCH23390 decreased coherence throughout the theta band, compared to vehicle ($P < 0.001$). SCH23390 had no effect on theta coherence between PL and BLA.

To determine if D1Rs modulate gamma oscillations in this circuit before CFC, we examined the acute effects of SCH23390 on gamma power in each area (Fig. 2C). Differences between SCH23390 and vehicle treatment in power at each individual frequency throughout the low and high gamma bands were quantified using a log ratio test. No obvious peak frequencies were observed for gamma power in any area in vehicle-treated controls. In DH, there was no effect of SCH23390 on gamma power. The largest effect of SCH23390 on gamma power

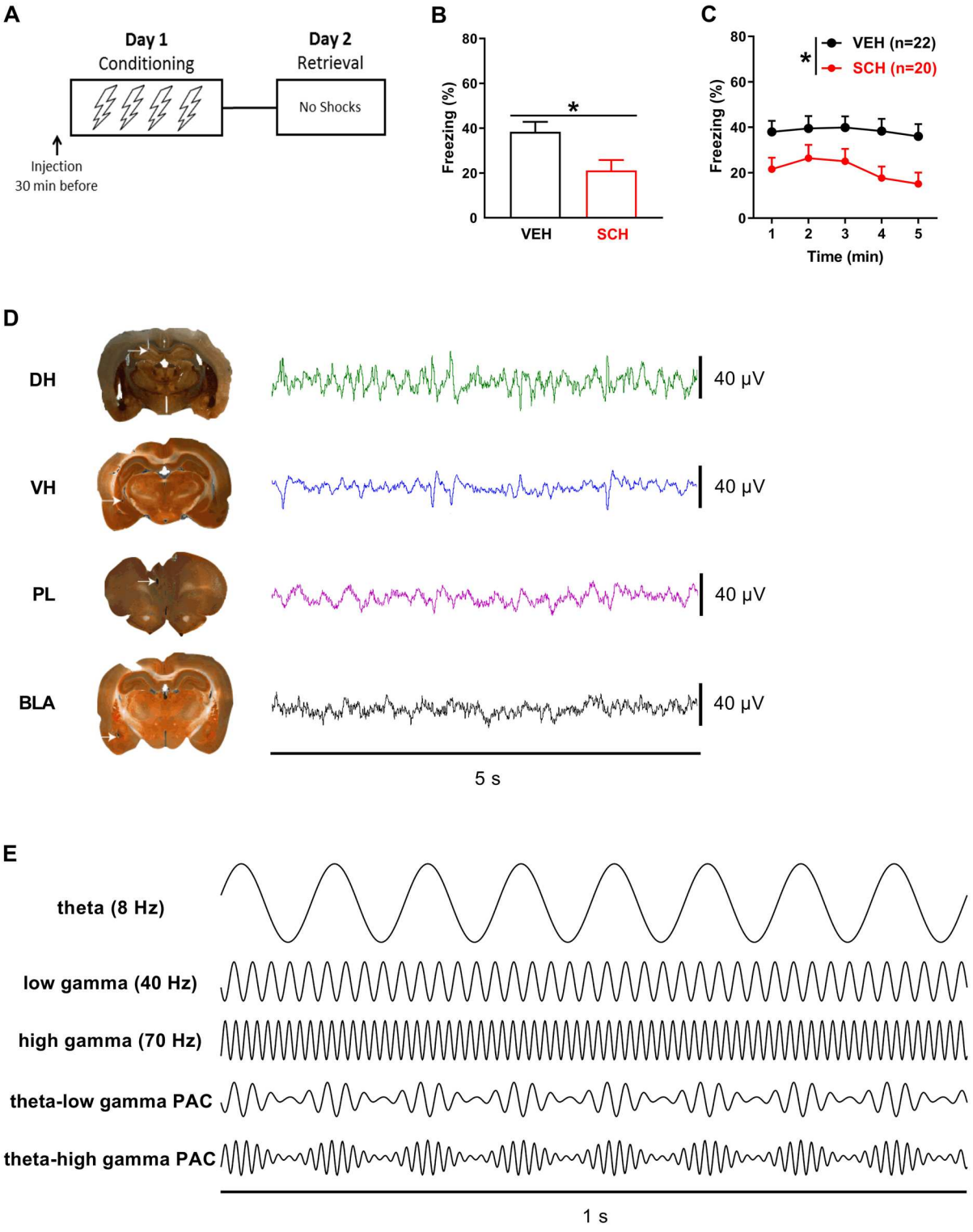

Figure 1. D1R blockade impairs CFC. (**A**) Schematic representation of the behavioral testing paradigm used. Rats received a systemic injection of SCH23390 (SCH) or vehicle (VEH) 30 min before conditioning, and LFPs were recorded during conditioning and retrieval testing. (**B**) SCH given before CFC decreased freezing at retrieval, compared to VEH (*$P < 0.05$). (**C**) A time course analysis showed that SCH resulted in decreased freezing throughout retrieval, compared to VEH (*$P < 0.05$). (**D**) Illustrative examples of electrode placements in (left; white arrows) and LFP signals recorded from (right) DH, VH, PL, and BLA. (**E**) Schematic representations of theta (8 Hz), low gamma (40 Hz), and high gamma (70 Hz) oscillations, and theta-gamma PAC at the low and high gamma frequencies.

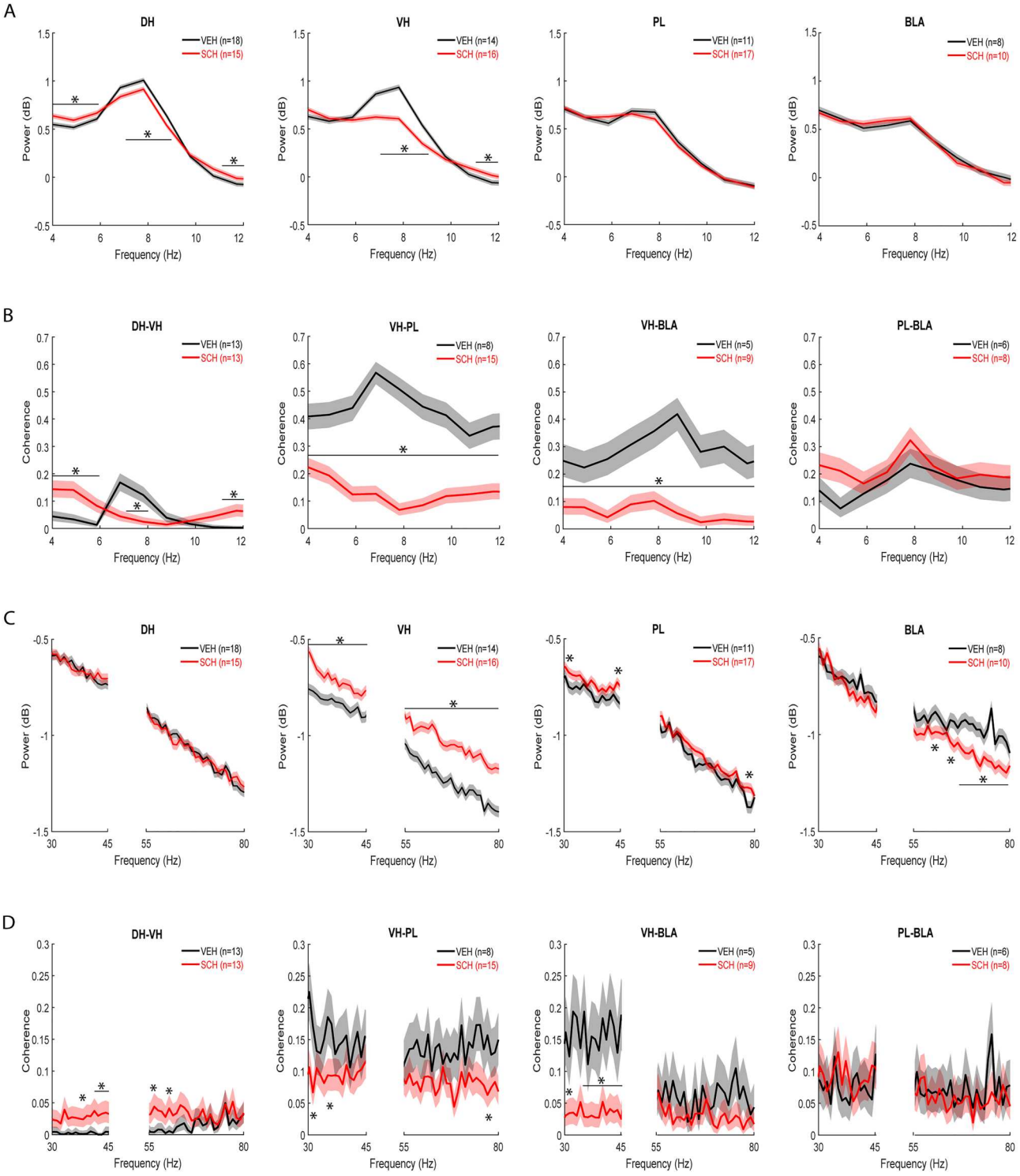

Figure 2. D1R blockade alters DH–VH and reduces VH–PL and VH–BLA synchrony before CFC. (**A**) Acute effects of SCH23390 (SCH) on theta power before CFC. Peak theta power occurred ~ 7–8 Hz in controls treated with vehicle (VEH). Compared to VEH, SCH decreased peak theta power and increased power outside the peak in DH and VH (*$P < 0.001$), but not PL or BLA. (**B**) Acute effects of SCH on theta coherence before CFC. Peak theta coherence occurred ~ 7–9 Hz with VEH. Compared to VEH, SCH decreased DH–VH peak theta coherence and increased DH–VH coherence outside the peak (*$P < 0.001$). SCH decreased VH–PL and VH–BLA theta coherence, compared to VEH (*$P < 0.001$), without affecting PL–BLA theta coherence. (**C**) Acute effects of SCH on gamma power before CFC. SCH had no effect on gamma power in DH. Compared to VEH, SCH increased gamma power in VH and PL (*$P < 0.001$). SCH decreased high gamma power in BLA, compared to VEH (*$P < 0.001$). (**D**) Acute effects of SCH on gamma coherence before CFC. SCH increased DH-VH and decreased VH–PL gamma coherence, compared to VEH (*$P < 0.001$). SCH decreased VH–BLA low gamma coherence, compared to VEH (*$P < 0.001$), without affecting PL–BLA gamma coherence.

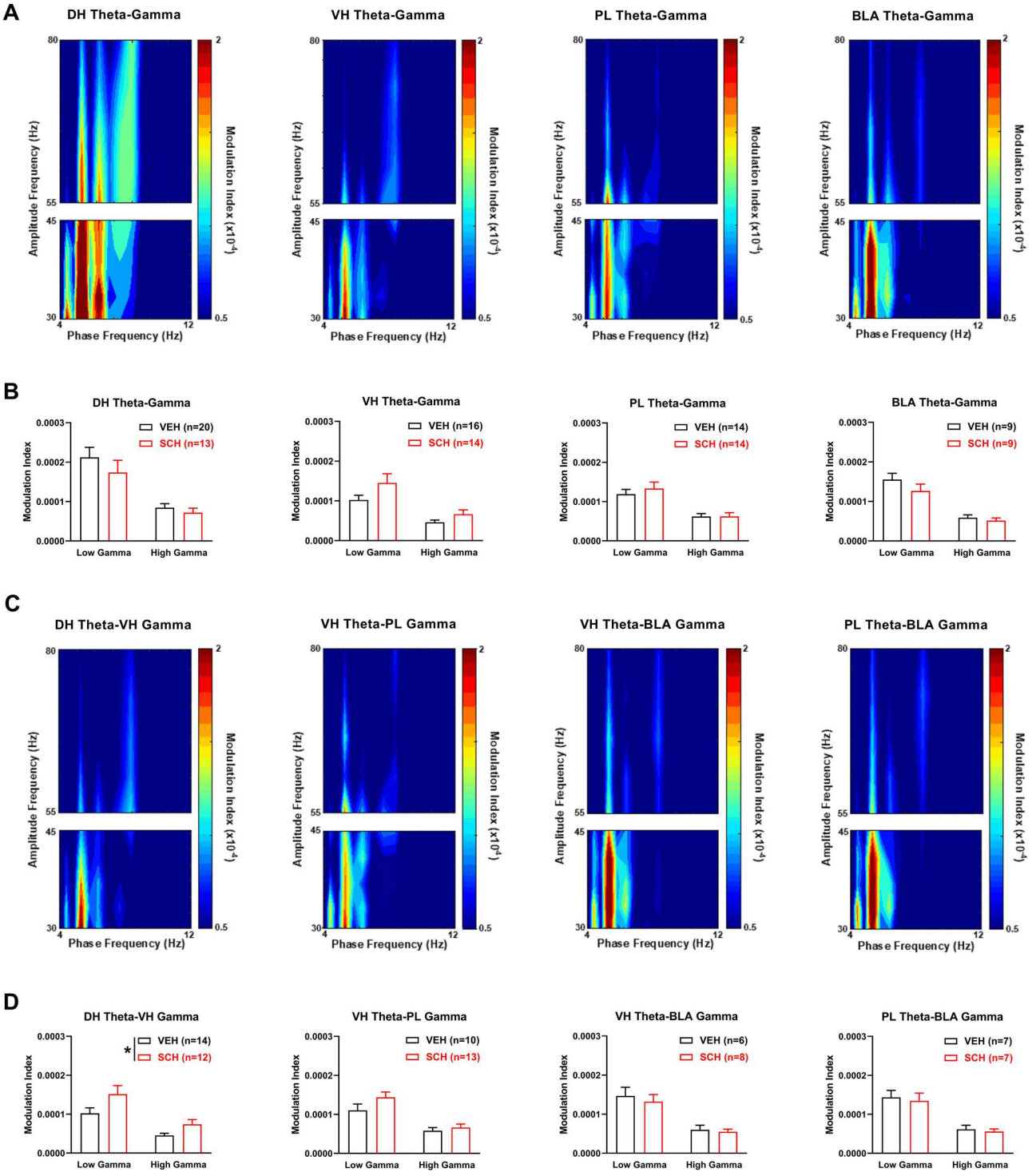

Figure 3. D1R blockade enhances theta-gamma coupling between DH and VH before CFC. (**A**) Theta-gamma PAC in each area after vehicle (VEH) treatment, with blue and red indicating lower and higher gamma amplitude, respectively. Peak PAC occurred at a theta frequency ~ 5 Hz in each area. (**B**) SCH23390 (SCH) had no effects on theta-gamma PAC in DH, VH, PL or BLA. (**C**) Theta-gamma PAC between areas with VEH, showing that peak PAC occurred ~ 5 Hz. (**D**) SCH increased DH theta coupling of VH gamma, compared to VEH (*$P < 0.05$). SCH had no effects on VH theta-PL gamma, VH theta-BLA gamma, or PL theta-BLA gamma PAC.

was observed in VH, where power was increased throughout the low and high gamma bands, compared to vehicle ($P < 0.001$). In PL, SCH23390 increased power at some low (31–32 and 44–45 Hz) and high (78–79 Hz) gamma frequencies, compared to vehicle ($P < 0.001$). In BLA, SCH23390 had no effect on low gamma power

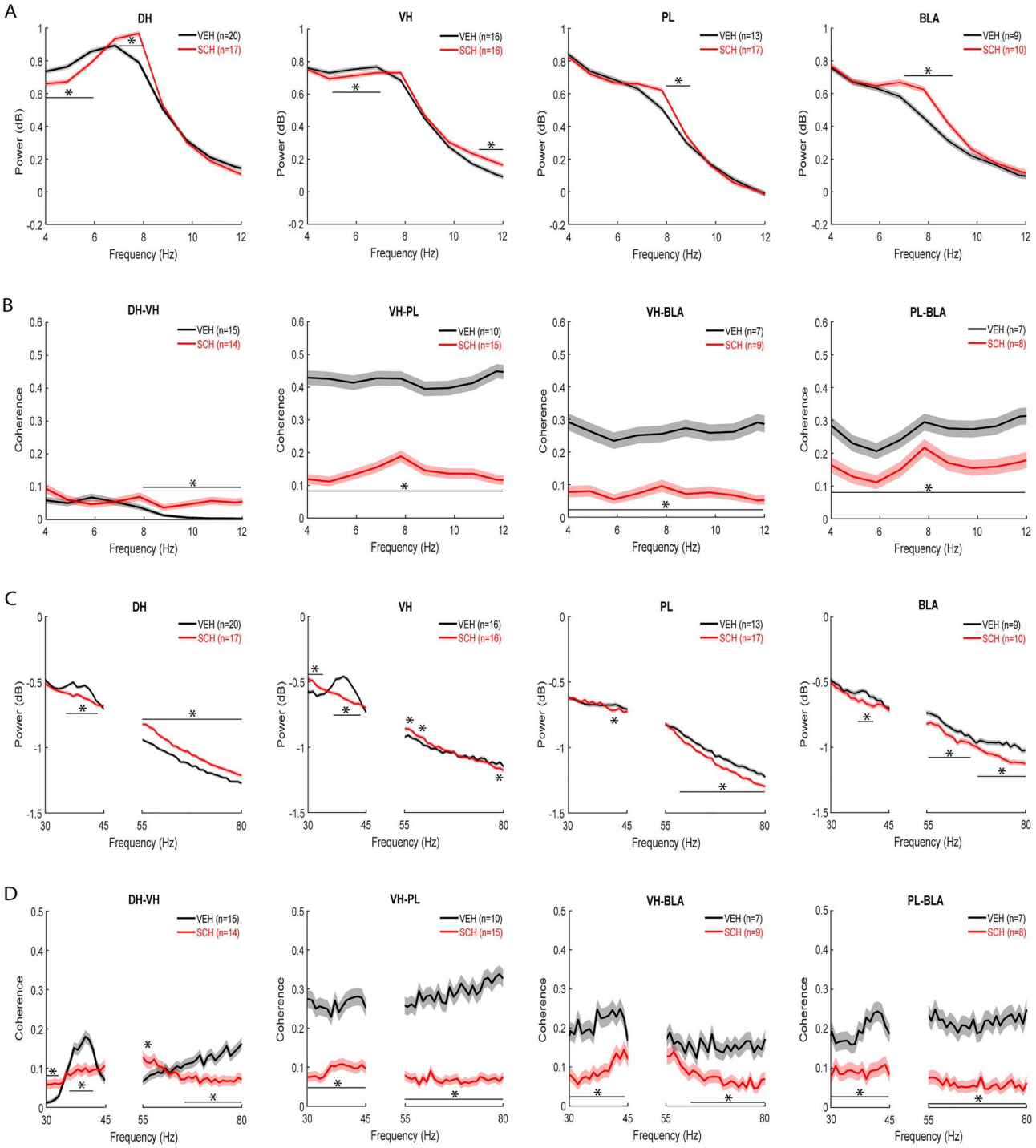

Figure 4. Impaired CFC by D1R blockade is associated with altered DH-VH and reduced VH–PL–BLA synchrony at retrieval. (**A**) Effects of SCH23390 (SCH) given before CFC on theta power at retrieval. Peak theta power occurred ~ 6–7 Hz in controls treated with vehicle (VEH), while SCH shifted the peak to ~ 7–8 Hz. In DH, SCH decreased lower and increased peak theta power, compared to VEH (*P < 0.001). In VH, SCH decreased lower and increased higher theta power, compared to VEH (*P < 0.001). In PL and BLA, SCH increased theta power, compared to VEH (*P < 0.001). (**B**) Effects of SCH given before CFC on theta coherence at retrieval. SCH increased DH–VH and decreased VH–PL, VH–BLA, and PL–BLA theta coherence, compared to VEH (*P < 0.001). (**C**) Effects of SCH given before CFC on gamma power at retrieval. A peak in low gamma power occurred ~ 35–40 Hz in DH, VH, and BLA, but not PL, with VEH. In DH, SCH decreased low and increased high gamma power, compared to VEH (*P < 0.001). In VH, SCH decreased peak low gamma power and increased low gamma power outside the peak, while increasing or decreasing power at various high gamma frequencies, compared to VEH (*P < 0.001). In PL and BLA, SCH decreased gamma power, compared to VEH (*P < 0.001). (**D**) Effects of SCH given before CFC on gamma coherence at retrieval. Peak low gamma coherence between DH and VH occurred at 35–40 Hz with VEH, but no peaks were observed for coherence between the other areas. SCH decreased DH–VH peak low gamma coherence and increased low gamma coherence outside the peak, while increasing or decreasing coherence at various high gamma frequencies, compared to VEH (*P < 0.001). SCH decreased VH–PL, VH–BLA, and PL–BLA gamma coherence, compared to VEH (*P < 0.001).

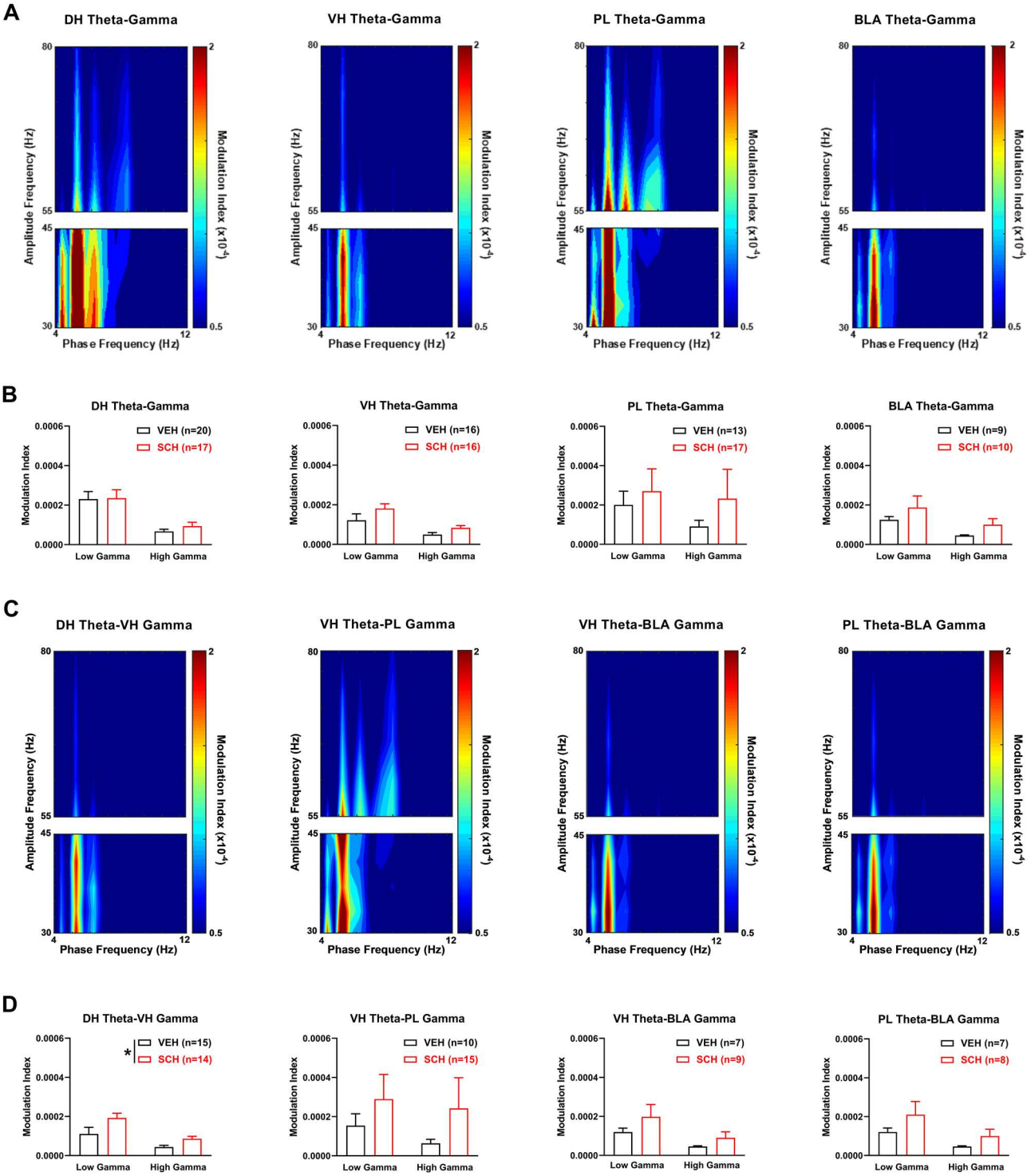

Figure 5. Impaired CFC by D1R blockade is associated with enhanced theta-gamma coupling between DH and VH at retrieval. (**A**) Theta-gamma PAC in each area after prior vehicle (VEH) treatment, with lower and higher gamma amplitude indicated by blue and red, respectively. Peak PAC occurred ~ 5 Hz in each area. (**B**) SCH23390 (SCH) given before CFC had no effects on theta-gamma PAC in DH, VH, PL or BLA. (**C**) Theta-gamma PAC between areas with prior VEH treatment, showing that peak PAC occurred ~ 5 Hz. (**D**) SCH given before CFC increased DH theta phase coupling of gamma amplitude in VH, compared to VEH (*P < 0.05). SCH given before CFC had no effects on VH theta-PL gamma, VH theta-BLA gamma, or PL theta-BLA gamma PAC.

and decreased high gamma power at various frequencies (60–61, 64–65, and 67–79 Hz, compared to vehicle ($P < 0.001$).

To determine if D1Rs modulate gamma synchrony before CFC, we examined the acute effects of SCH23390 on gamma coherence in this circuit (Fig. 2D). Differences between SCH23390 and vehicle treatment in coherence

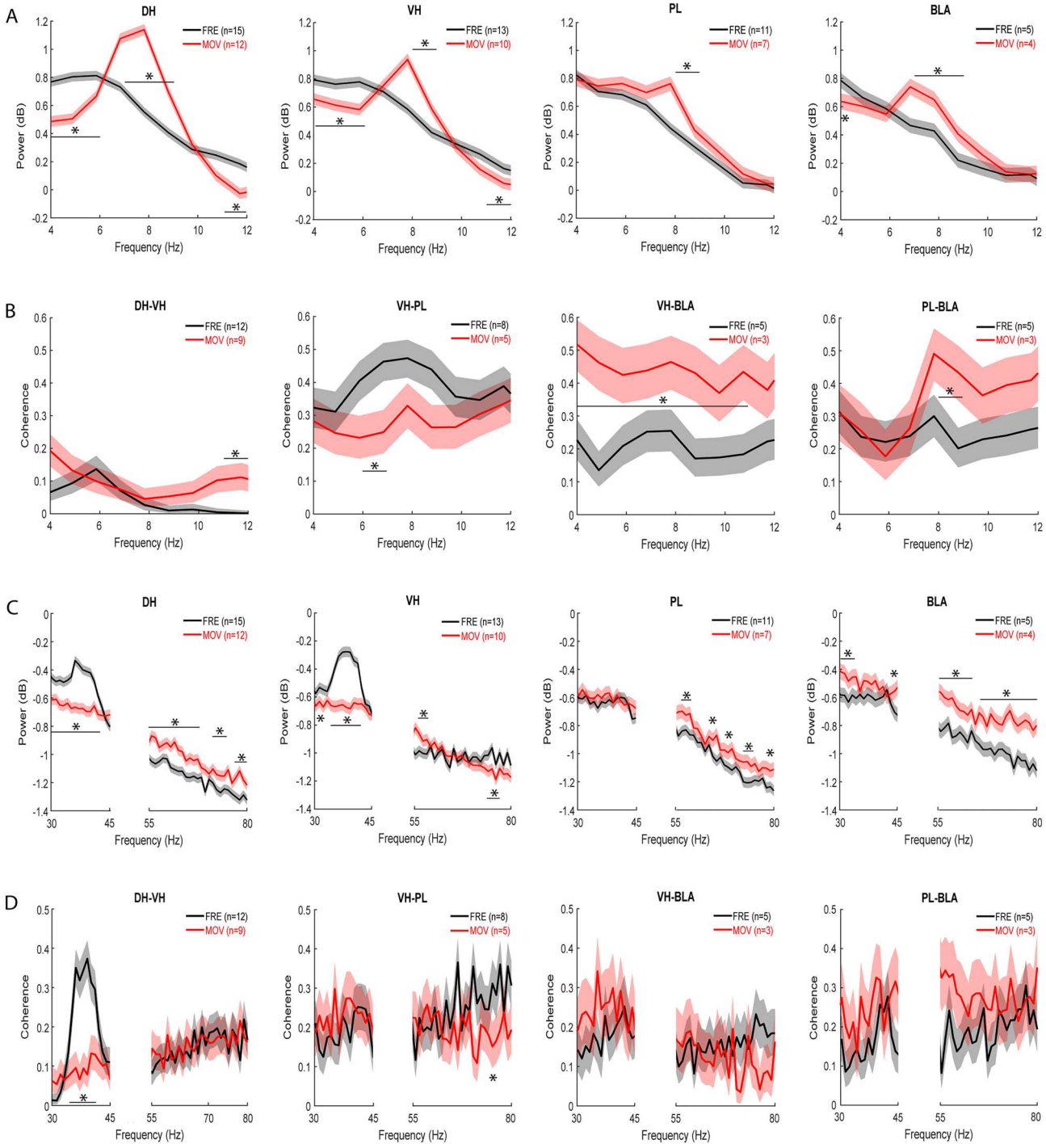

Figure 6. Movement and freezing in vehicle-treated controls are associated with differences in DH–VH and VH–PL–BLA synchrony at retrieval. (**A**) Differences between movement (MOV) and freezing (FRE) in theta power at retrieval. Peak theta power occurred ~ 7–8 Hz with MOV. Compared to FRE, MOV increased peak theta power and decreased theta power outside the peak in DH and VH (*$P < 0.001$). In PL and BLA, MOV increased theta power, compared to FRE (*$P < 0.001$). (**B**) Differences between MOV and FRE in theta coherence at retrieval. Compared to FRE, MOV increased DH–VH, VH–BLA, and PL–BLA theta coherence (*$P < 0.001$). MOV decreased VH–PL theta coherence, compared to FRE (*$P < 0.001$). (**C**) Differences between MOV and FRE in gamma power at retrieval. A peak in low gamma power occurred ~ 35–40 Hz with FRE in DH and VH, but not PL or BLA. In DH, MOV decreased low and increased high gamma power, compared to FRE (*$P < 0.001$). In VH, MOV decreased low gamma power, while power was increased or decreased at various high gamma frequencies, compared to FRE (*$P < 0.001$). In PL, MOV increased high gamma power, compared to FRE (*$P < 0.001$). In BLA, MOV increased gamma power, compared to FRE (*$P < 0.001$). (**D**) Differences between MOV and FRE in gamma coherence at retrieval. Peak low gamma coherence between DH and VH occurred ~ 35–40 Hz with FRE, but there were no peaks for gamma coherence between other areas. MOV decreased DH-VH low gamma coherence, compared to FRE (*$P < 0.001$). MOV decreased VH–PL high gamma coherence, compared to FRE (*$P < 0.001$). MOV had no effects on VH–BLA or PL–BLA gamma coherence.

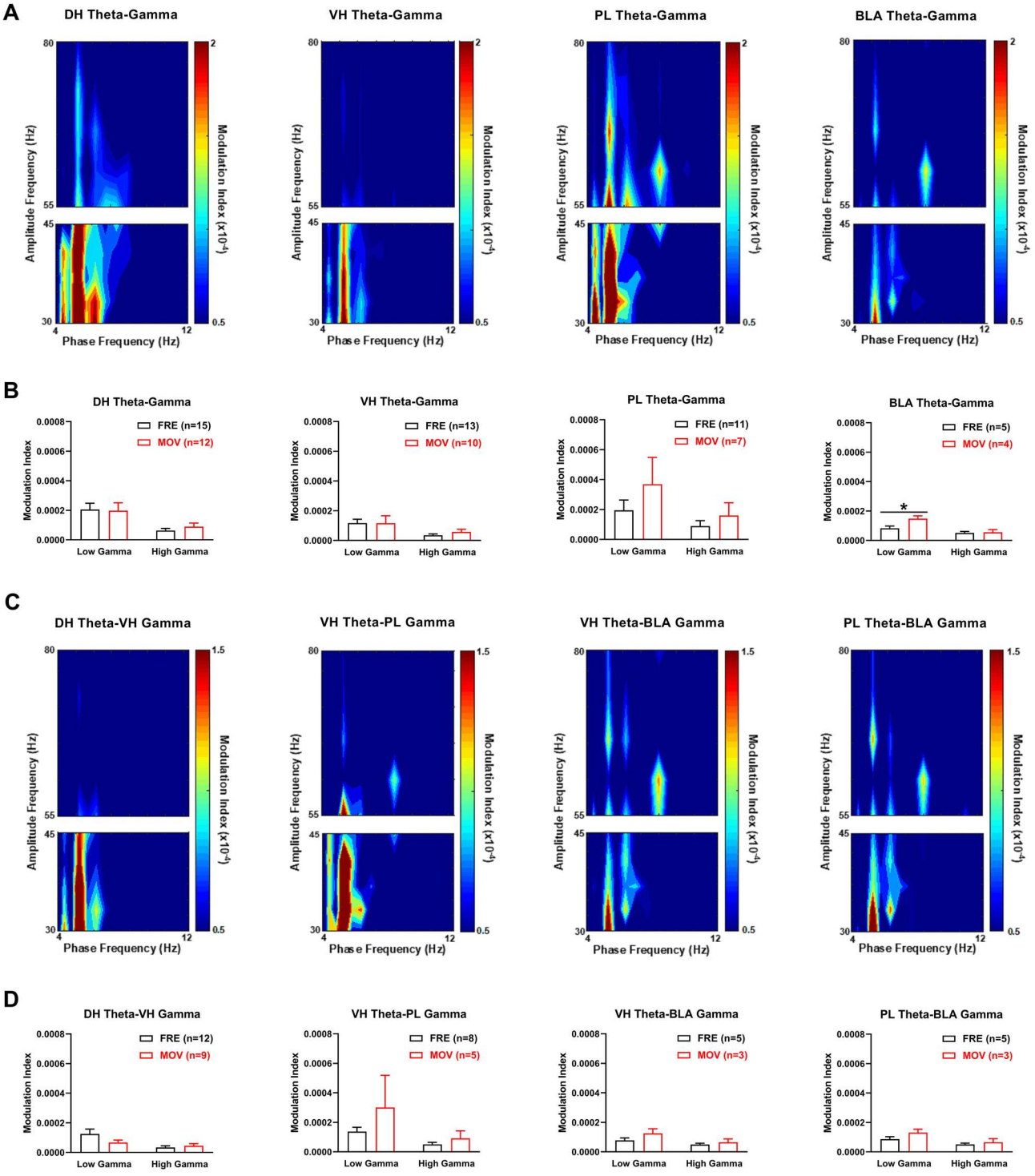

Figure 7. Movement in vehicle-treated controls enhances theta-gamma coupling in BLA at retrieval. (**A**) Theta-gamma PAC in each area during freezing (FRE), with lower and higher gamma amplitude indicated by blue and red, respectively. Peak PAC occurred ~ 5 Hz in each area. (**B**) Movement (MOV) had no effect on theta-gamma PAC in DH, VH, or PL. MOV increased theta coupling of low gamma in BLA, compared to FRE (*$P < 0.05$). (**C**) Theta-gamma PAC between areas during FRE, showing that peak PAC occurred ~ 5 Hz. (**D**) MOV had no effects on DH theta–VH gamma, VH theta–PL gamma, VH theta–BLA gamma, or PL theta–BLA gamma PAC.

were quantified at each individual frequency throughout the low and high gamma bands using a chi-squared difference of coherence test. There were no obvious peak frequencies observed for gamma coherence in vehicle-treated controls. SCH23390 increased coherence between DH and VH at low (37–39 and 41–45 Hz) and high

(56–57 and 60–62 Hz) gamma frequencies, compared to the low levels of gamma coherence observed with vehicle ($P < 0.001$). In contrast, coherence between VH and PL was decreased by SCH23390 at some low (30–31 and 35–36 Hz) and high (74–75 Hz) gamma frequencies, compared to vehicle ($P < 0.001$). SCH23390 also decreased gamma coherence between VH and BLA at low (30–33 and 35–45 Hz; $P < 0.001$) but not high gamma frequencies, compared to vehicle. SCH23390 had no effect on gamma coherence between PL and BLA, compared to vehicle.

To determine if D1Rs modulate theta-gamma coupling in this circuit before CFC, we examined the acute effects of SCH23390 on theta-gamma phase-amplitude coupling (PAC) in each area (Fig. 3A,B). Theta-gamma PAC was quantified using a modulation index. Although peak theta power in each area occurred ~ 7–8 Hz (Fig. 2A), color plots of theta-gamma PAC in each area showed that peak theta phase coupling of gamma amplitude occurred ~ 5 Hz with vehicle (Fig. 3A) or SCH23390 (not shown). Therefore we focused the analysis on this theta frequency. The quantitative analysis using two-way ANOVA found no acute effects of SCH23390 on theta-gamma PAC in any area (Fig. 3B and Table S1).

We also examined the acute effects of SCH23390 on theta-gamma PAC between the directly inter-connected areas before CFC (Fig. 3C,D). Color plots of theta-gamma PAC between areas showed that peak PAC occurred ~ 5 Hz with vehicle (Fig. 3C) or SCH23390 (not shown), therefore the analysis was focused on this theta frequency. Compared to vehicle, SCH23390 increased DH theta coupling of VH gamma (Fig. 3D). Two-way ANOVA revealed a significant main effect of treatment ($F_{(1,24)} = 4.41$, $P = 0.046$) but no treatment x frequency interaction ($F_{(1,24)} = 1.75$, $P = 0.20$). For VH theta coupling of PL gamma, two-way ANOVA found no main effect of treatment ($F_{(1,21)} = 1.61$, $P = 0.22$) but revealed a significant treatment x frequency interaction ($F_{(1,21)} = 4.53$, $P = 0.045$); however, post-hoc testing found no difference between vehicle and SCH23390 treatment at low or high gamma frequencies. There were also no effects of SCH23390 on VH or PL theta coupling of BLA gamma (Table S1).

Impaired CFC by D1R blockade is associated with altered intra-hippocampal and reduced hippocampal–prefrontal–amygdala synchrony at retrieval

To determine the association between hippocampal–prefrontal–amygdala theta oscillations and contextual fear memory, we examined the effects of impaired CFC by prior SCH23390 administration on theta power in each area during later retrieval tested drug-free (Fig. 4A). Compared to theta power before CFC, there was less of a peak that was shifted to 6–7 Hz in hippocampus, with much less prominent peaks in PL or BLA, in vehicle-treated controls. Overall, SCH23390 shifted the peak to 7–8 Hz in each area. SCH23390 resulted in the biggest increase in peak theta power in DH (7–8 Hz), while also decreasing power at lower frequencies (4–6 Hz), compared to vehicle ($P < 0.001$). In VH, SCH23390 decreased power at lower (5–7 Hz) and increased power at higher (11–12 Hz) theta frequencies, compared to vehicle ($P < 0.001$). SCH23390 increased peak theta power in PL (8–9 Hz) and BLA (7–9 Hz), compared to vehicle ($P < 0.001$).

To determine the association between theta synchrony and contextual fear memory, we examined the effects of impaired CFC by prior SCH23390 administration on theta coherence in this circuit at retrieval (Fig. 4B). Compared to theta power, peaks for theta coherence were less pronounced or absent. Overall, SCH23390 increased theta coherence within hippocampus and decreased theta coherence between VH, PL, and BLA. SCH23390 increased coherence between DH and VH at higher theta frequencies (8–12 Hz), compared to vehicle ($P < 0.001$). In contrast, SCH23390 caused a large decrease in VH–PL, VH–BLA, and PL–BLA coherence throughout the theta band, compared to vehicle ($P < 0.001$).

To determine the association between gamma oscillations and contextual fear memory, we examined the effects of impaired CFC by prior SCH23390 administration on gamma power in each area at retrieval (Fig. 4C). Compared to low gamma power before CFC, there was a peak at 35–40 Hz in hippocampus and, to a lesser extent, in BLA and PL in vehicle-treated controls. In DH, SCH23390 decreased peak low gamma power (35–43 Hz) and increased power throughout the high gamma band, compared to vehicle ($P < 0.001$). In VH, SCH23390 decreased peak low gamma power (36–43 Hz) but increased low gamma power outside the peak (30–34 Hz), while increasing power at some (55–57 and 59–60 Hz) and decreasing power at other (78–79 Hz) high gamma frequencies, compared to vehicle ($P < 0.001$). In PL, SCH23390 decreased power at some low (41–42 Hz) and most high (58–80 Hz) gamma frequencies, compared to vehicle ($P < 0.001$). In BLA, SCH23390 decreased peak low gamma power (37–41 Hz) and high gamma power at most frequencies (55–66 and 68–80 Hz), compared to vehicle ($P < 0.001$).

To determine the association between gamma synchrony and contextual fear memory, we examined the effects of impaired CFC by prior SCH23390 administration on gamma coherence in this circuit at retrieval (Fig. 4D). Vehicle-treated controls showed a peak for low gamma coherence within hippocampus at 35–40 Hz but there were no obvious peaks observed for gamma coherence between any other areas. SCH23390 decreased peak low gamma coherence between DH and VH (36–42 Hz) and increased low gamma coherence outside the peak (30–33 Hz), while increasing coherence at some (55–56 Hz) and decreasing coherence at other (65–80 Hz) high gamma frequencies, compared to vehicle ($P < 0.001$). SCH23390 caused a large decrease in coherence between VH and PL throughout the low and high gamma bands, compared to vehicle ($P < 0.001$). SCH23390 also decreased coherence between VH and BLA at most low (30–44 Hz) and high (61–80 Hz) gamma frequencies, compared to vehicle ($P < 0.001$). Similarly, SCH23390 resulted in a large decrease in coherence between PL and BLA across the low and high gamma bands, compared to vehicle ($P < 0.001$).

To determine the association between theta-gamma coupling and contextual fear memory, we examined the effects of impaired CFC by prior SCH23390 administration on theta-gamma PAC in each area at retrieval (Fig. 5A,B). Color plots of theta-gamma PAC in each area showed that peak PAC occurred ~ 5 Hz with vehicle (Fig. 5A) or SCH23390 (not shown), thus we focused the analysis on this frequency. The quantitative analysis

found no effects of impaired CFC by SCH23390 on theta-gamma PAC in any area at retrieval (Fig. 5B and Table S2).

We also examined the effects of impaired CFC by prior SCH23390 administration on theta-gamma PAC between these areas at retrieval (Fig. 5C,D). Color plots of theta-gamma PAC between areas showed that peak PAC occurred ~ 5 Hz with vehicle (Fig. 5C) or SCH23390 (not shown), therefore we focused the analysis on this frequency. Compared to vehicle, SCH23390 increased DH theta coupling of VH gamma (Fig. 5D). Two-way ANOVA revealed a significant main effect of treatment ($F_{(1,27)} = 5.03$, $P = 0.033$) but no treatment × frequency interaction ($F_{(1,27)} = 1.70$, $P = 0.20$). SCH23390 had no effects on VH theta coupling of gamma in PL or BLA; similarly, there was no effect of SCH23390 on PL theta coupling of BLA gamma (Table S2).

Reduced hippocampal–prefrontal–amygdala synchrony associated with impaired CFC by D1R blockade is not fully accounted for by increased movement at retrieval

Because theta and gamma oscillations in these areas are associated with movement[45–47], and contextual fear was inferred from freezing, we also compared synchronized oscillations between epochs of movement and freezing during retrieval testing in the vehicle-treated controls. We reasoned that if the reduced freezing and associated oscillatory synchrony resulting from SCH23390 given before CFC simply reflected increased movement at retrieval then we would find a similar synchrony profile with movement, compared to freezing, in the controls at retrieval. However, if we found differences between these synchrony profiles then this may instead reflect different neural signatures for movement and contextual fear memory.

In terms of hippocampal–prefrontal–amygdala theta oscillations in the controls at retrieval, movement was associated with a peak in theta power at 7–8 Hz in each area (Fig. 6A). In DH, movement increased peak theta power (7–9 Hz) and decreased theta power outside the peak (4–6 and 11–12 Hz), compared to freezing ($P < 0.001$). In VH, movement also increased peak theta power (8–9 Hz), while theta power was also decreased outside the peak (4–6 and 11–12 Hz), compared to freezing ($P < 0.001$). Movement increased peak theta power in PL (8–9 Hz) and BLA (7–9 Hz), compared to freezing ($P < 0.001$).

In terms of theta synchrony in this circuit in the controls at retrieval, there were less obvious peaks in theta coherence with movement in comparison to theta power (Fig. 6B). Movement increased coherence between DH and VH at higher theta frequencies (11–12 Hz), compared to freezing ($P < 0.001$). In contrast, movement decreased peak theta coherence (6–7 Hz) between VH and PL, compared to freezing ($P < 0.001$). Movement increased coherence between VH and BLA across most theta frequencies (4–11 Hz), compared to freezing ($P < 0.001$). Movement also increased peak theta coherence (8–9 Hz) between PL and BLA, compared to freezing ($P < 0.001$).

In terms of gamma oscillations in this circuit in the controls at retrieval, freezing was associated with a peak in low gamma power at 35–40 Hz in hippocampus, but not in PL or BLA (Fig. 6C). In DH, movement decreased low (30–42 Hz) and increased high (55–67, 71–75, and 77–80 Hz) gamma power, compared to freezing ($P < 0.001$). In VH, movement also decreased low gamma power (30–32 and 34–42 Hz), while power was increased (56–59 Hz) or decreased (74–77 Hz) at various high gamma frequencies, compared to freezing ($P < 0.001$). In PL, movement had no effect on low and increased high gamma power (56–59, 64–65, 67–69, 72–75, and 78–80), compared to freezing ($P < 0.001$). In BLA, movement increased both low (30–34 and 44–45 Hz) and high (55–63 and 65–80 Hz) gamma power, compared to freezing ($P < 0.001$).

In terms of gamma synchrony in this circuit in the controls at retrieval, freezing was associated with a peak in low gamma coherence at 35–40 Hz within hippocampus but not between any other areas (Fig. 6D). Movement abolished peak low gamma coherence between DH and VH (35–41 Hz; $P < 0.001$) but had no effect on high gamma coherence, compared to freezing. Movement had no effect on low gamma coherence between VH and PL but decreased coherence at some high gamma frequencies (70–71 Hz), compared to freezing ($P < 0.001$). Movement had no effect on gamma coherence between VH and BLA, or between PL and BLA.

In terms of theta-gamma coupling in this circuit in the controls at retrieval, color plots of theta-gamma PAC in each area showed that peak PAC occurred ~ 5 Hz with freezing (Fig. 7A) or movement (not shown), therefore the analysis was focused on this frequency. The quantitative analysis found no differences between movement and freezing in DH, VH, or PL (Fig. 7B and Table S3). However, compared to freezing, movement increased theta coupling of low gamma in BLA. Two-way ANOVA showed no main effect of locomotion ($F_{(1,7)} = 4.05$, $P = 0.084$) but revealed a marginally significant locomotion × frequency interaction ($F_{(1,7)} = 5.59$, $P = 0.050$). Post-hoc testing confirmed that theta coupling of low gamma was significantly increased with movement, compared to freezing ($P < 0.05$).

We also examined differences between movement and freezing in theta-gamma coupling between these areas in the controls at retrieval (Fig. 7C,D). Color plots of theta-gamma PAC between areas showed that peak PAC occurred ~ 5 Hz with freezing (Fig. 7C) or movement (not shown), therefore we focused our analysis at this frequency. The quantitative analysis found no differences between movement and freezing on theta-gamma PAC between any areas at retrieval (Fig. 7D and Table S3). For DH theta coupling of VH gamma, two-way ANOVA found no main effect of locomotion ($F_{(1,19)} = 0.69$, $P = 0.42$) but revealed a significant locomotion × frequency interaction ($F_{(1,19)} = 4.97$, $P = 0.038$); however, post-hoc testing found no difference between movement and freezing at low or high gamma frequencies.

Discussion

We determined the effects of systemic D1R blockade on CFC and associated synchronized oscillations in the hippocampal–prefrontal–amygdala circuit. The selective D1R antagonist SCH23390 impaired CFC and acted acutely to alter intra-hippocampal and reduce hippocampal-prefrontal and hippocampal-amygdala synchrony during conditioning. SCH23390 decreased peak theta coherence and increased gamma coherence and theta-gamma PAC

between DH and VH, while VH-PL and VH-BLA theta and gamma coherence were decreased. Impaired CFC by SCH23390 was associated with altered intra-hippocampal and reduced hippocampal–prefrontal–amygdala synchrony at retrieval. Prior SCH23390 decreased peak low gamma coherence and increased theta coherence and theta-gamma PAC between DH and VH, while resulting in decreased VH–PL, VH–BLA, and PL–BLA theta and gamma coherence (Fig. 8). This reduction in hippocampal–prefrontal–amygdala synchrony was not fully accounted for by non-specific increases in movement occurring with decreased freezing at retrieval. This was revealed by comparing between epochs of movement and freezing in the vehicle-treated controls, which showed that movement increased VH–BLA and PL–BLA theta coherence and had no effect on VH–BLA or PL–BLA gamma coherence (Table 1). These results provide evidence that D1R signalling regulates CFC by modulating synchronized oscillations in the hippocampal–prefrontal–amygdala circuit, which also reflect a neural signature of contextual fear memory.

Our finding that SCH23390 impaired CFC, as indicated by decreased freezing at retrieval in comparison to vehicle, replicates our previous results[23,24]. In those studies, we showed that SCH23390 impairs the acquisition, but not consolidation, of contextual fear since SCH23390 given before, but not immediately after, conditioning

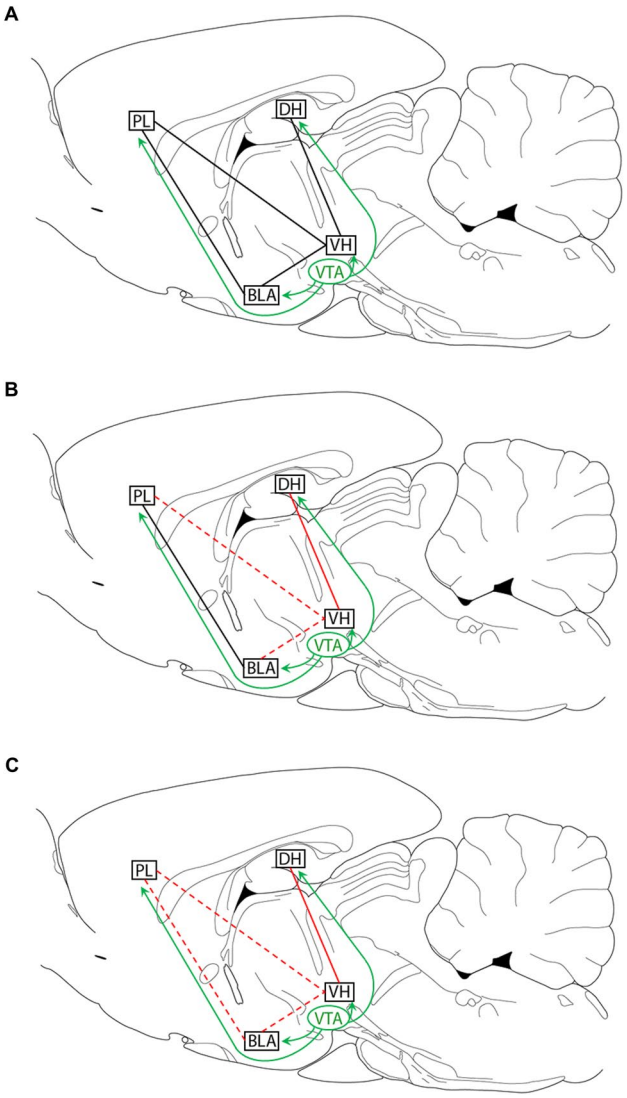

Figure 8. Summary of the key effects of D1R blockade before CFC on hippocampal–prefrontal–amygdala synchrony before conditioning and at retrieval tested drug-free. (**A**) Dopamine projections from the ventral tegmental area (VTA) to DH, PL, and BLA (green lines) regulate CFC and local synaptic plasticity via D1R signalling. DH projects to PL and BLA indirectly through VH (black lines). (**B**) SCH23390 acts acutely before conditioning to alter intra-hippocampal (solid red line; decreased peak theta coherence, increased gamma coherence and theta-gamma PAC) and reduce hippocampal-prefrontal and hippocampal–amygdala (dashed red lines; decreased theta and gamma coherence) synchrony. (**C**) Impaired CFC by SCH23390 is associated with altered intra-hippocampal (solid red line; decreased gamma coherence, increased theta coherence and theta-gamma PAC) and reduced hippocampal–prefrontal–amygdala (dashed red lines; decreased theta and gamma coherence) synchrony at retrieval.

reduced freezing at retrieval. Moreover, this effect of SCH23390 did not involve state dependency, acute drug effects on shock sensitivity during conditioning, or lasting drug effects on locomotion at retrieval 24 h later. This latter finding is in keeping with the brief (~ 25 min) half-life of SCH23390 in rats[48]. Taken together, these results indicate that D1R signalling at the time of conditioning is important for contextual fear learning.

Systemic or local D1R blockade has acute effects on hippocampal[34–38], prefrontal[39,40], and amygdala[41] oscillations. However, less is known about D1R modulation of synchronized oscillations between these inter-connected areas. Intra-cerebroventricular SCH23390 infusion reduces theta phase synchrony between VH and PL under anesthesia[36]. SCH23390 infused into VH prevents the increase in phase-locking of PFC spike firing to VH theta that occurs during learning[37]. Our results showing that SCH23390 decreased theta and gamma coherence between VH and PL before CFC broadly agrees with these previous findings. We also found that SCH23390 decreased theta and gamma coherence between VH and BLA before CFC without affecting PL–BLA synchrony. In contrast, the effects of SCH23390 on DH–VH synchrony were more complex. SCH23390 decreased peak theta coherence but increased gamma coherence and theta-gamma PAC. This suggests that D1R signalling has different effects on the modulation of intra-hippocampal coupling and synchrony between hippocampus and its projection areas.

Our finding that impaired CFC by SCH23390 was characterized by reduced hippocampal–prefrontal–amygdala synchrony at retrieval generally agrees with evidence indicating that synchronized oscillations in this circuit are crucial for fear memory. Theta synchrony between hippocampus and PFC[49] or amygdala[50–52] is enhanced during contextual fear retrieval. Moreover, hippocampal–amygdala theta synchrony is associated with long-term (24 h) but not short-term (30 min) contextual fear memory or fear expression per se. We examined VH–PL and VH–BLA synchrony since hippocampal projections to these areas occur through VH[10,11,13]. Our results showing that impaired CFC is associated with reduced VH-PL and VH-BLA theta coherence at retrieval confirm and extend these previous findings implicating hippocampal-prefrontal and hippocampal–amygdala theta synchrony in contextual fear memory. Our finding of reduced PL–BLA theta coherence with impaired CFC also broadly agrees with studies showing that prefrontal–amygdala theta synchrony is involved in auditory fear retrieval[53,54]. Similarly, we found reduced VH–PL, VH–BLA, and PL–BLA gamma coherence at retrieval with impaired CFC, suggesting that gamma synchrony between these areas also plays a role in contextual fear retrieval. This is compatible with evidence indicating that BLA gamma oscillations are important for contextual memory consolidation and that gamma coherence between BLA and various inter-connected areas is enhanced during learning[55–57]. However, impaired CFC was associated with more complex interactions between DH and VH at retrieval. While peak low gamma coherence between DH and VH was decreased, theta and higher gamma coherence and theta-gamma PAC were increased. This suggests that impaired CFC is characterized by differences in intra-hippocampal coupling and hippocampal-prefrontal–amygdala synchrony at retrieval.

A potential confounding issue for interpreting the effects of systemic D1R blockade on hippocampal–prefrontal–amygdala synchrony is that non-specific locomotor effects might be involved. SCH23390 acts acutely to decrease locomotion[22,23], while decreased freezing at retrieval resulting from impaired CFC by SCH23390 has the opposite effect to increase movement. Therefore opposing effects of SCH23390 acutely and during later retrieval might be expected if non-specific locomotor effects are involved. Although SCH23390 had the opposite effects on peak theta and low gamma coherence between DH and VH acutely and at retrieval, there were similar effects on DH-VH theta-gamma PAC, VH-PL theta and gamma coherence, and VH–BLA theta and gamma coherence under both conditions. To address this issue, we also compared hippocampal–prefrontal–amygdala synchrony between epochs of movement and freezing at retrieval in the vehicle-treated controls. If reduced freezing and VH–PL–BLA synchrony with impaired CFC by SCH23390 reflected a non-specific increase in locomotion at retrieval, then we expected to find a similar synchrony profile with movement in the controls, whereas differences between these synchrony profiles may indicate specific effects on contextual fear memory. Our results showed both similarities and differences in these synchrony profiles (Table 1). Movement increased theta and decreased peak low gamma coherence between DH and VH in controls, as we found with SCH23390. Movement

Areas	Synchrony measure	SCH23390	Movement
DH–VH	Theta coherence	↑	↑
	Gamma coherence	↓/↑	↓
	Theta-gamma PAC	↑	↔
VH–PL	Theta coherence	↓	↓
	Gamma coherence	↓	↓
	Theta-gamma PAC	↔	↔
VH–BLA	Theta coherence	↓	↑
	Gamma coherence	↓	↔
	Theta-gamma PAC	↔	↔
PL–BLA	Theta coherence	↓	↑
	Gamma coherence	↓	↔
	Theta-gamma PAC	↔	↔

Table 1. Comparison of effects of impaired CFC by SCH23390 versus movement in the vehicle-treated controls on hippocampal–prefrontal–amygdala synchrony at retrieval.

also decreased VH–PL theta and gamma coherence in controls, albeit to a lesser extent than with SCH23390. However, VH–BLA and PL–BLA theta coherence were increased with movement in controls but decreased with SCH23390. Movement also had no effects on VH–BLA or PL–BLA gamma coherence in controls, whereas SCH23990 resulted in decreased gamma coherence between these areas. These results suggest that while the effects of SCH23390 on DH–VH and VH–PL synchrony at retrieval may have involved non-specific increases in movement, BLA synchrony with VH and PL during retrieval was instead more likely to have reflected a neural signature of contextual fear memory.

In summary, this study lends support to the idea that D1Rs regulate CFC by modulating hippocampal–prefrontal–amygdala synchrony. Synaptic plasticity in this circuitry, which is disrupted by local D1R blockade[25–27], is facilitated by synchronized oscillations[28,30,32]. Reduced synchrony between these areas is therefore a plausible neurophysiological mechanism by which D1R blockade disrupts the synaptic plasticity underlying CFC. This has implications for understanding how the various psychological processes involved are mediated by communication between these areas. D1R blockade locally in DH impairs CFC and LTP in this area[23,25], which may interfere with encoding the context representation and context-US association. Although blocking D1Rs locally in VH does not affect CFC[24], our results suggest that altered synchrony between DH and VH by systemic D1R blockade may also play a role in disrupting CFC. Moreover, reduced VH–PL and VH–BLA synchrony with systemic D1R blockade may impair CFC by interfering with the context and US representations being conveyed from hippocampus to these areas[13,15]. In support of this idea, blocking D1Rs locally in PL impairs CFC and LTP in the VH–PL pathway[24,26]. Local D1R blockade in BLA also impairs CFC and LTP in this area[23,27], which may interfere with encoding the US representation and context-US association[58]. However, D1R modulation of VH–BLA plasticity[14,59] remains to be determined. It is worth noting that other areas inter-connected to this circuit may also play a role in D1R modulation of hippocampal–prefrontal–amygdala synchrony. The thalamic nucleus reuniens (RE) mediates hippocampal-prefrontal coupling via its reciprocal connections with these areas[60], while the PFC–RE and RE–BLA pathways have been implicated in various learned fear processes[32,61–63]. Moreover, D1Rs in RE regulate fear extinction memory and dopamine modulates theta oscillations in RE[64,65], suggesting a potential role for RE in D1R modulation of synchrony in this circuit. Nevertheless, this study builds on our understanding of the hippocampal–prefrontal–amygdala circuit mechanisms underlying the neuromodulation of CFC by dopamine. It also confirms and adds to evidence indicating that communication within this circuitry is crucial for fear memory[28,30,32]. This may ultimately lead to novel insights on the neurobiological basis of anxiety-related disorders characterized by aberrant learned fear processing.

Methods

Animals

42 male Lister Hooded rats (Charles River, UK) weighing 280–390 g before surgery were used. Rats were group housed in individually ventilated cages (2–3/cage) and kept on a 24 h light/dark cycle (lights on at 7:00) with ad libitum access to food and water. All behavioral testing occurred during the rats' light cycle. All experimental procedures were performed with institutional ethical approval and under the UK Animals (Scientific Procedures) Act 1986 (Home Office Project Licence 30/3230). All experiments were performed in accordance with the relevant guidelines and regulations. All reporting for the study followed the recommendations in the ARRIVE guidelines (Essential 10;[66]).

Electrode implant surgery

Anesthesia was induced with ~ 3% isoflurane in oxygen and analgesic (buprenorphine, 0.05 mg/kg, s.c.) was administered immediately post-induction. Anesthesia was maintained with 1.5–2.5% isoflurane during surgery to ensure complete inhibition of the hindpaw withdrawal reflex. Rats were placed in a stereotaxic frame and the incisor bar was adjusted to maintain the skull horizontal. A homoeothermic heating pad was used to maintain body temperature at 36–37 °C throughout surgery. A scalp incision was made along the midline, the periosteum was retracted, and 10 stainless steel anchoring screws were affixed to the top and sides of the skull. Small craniotomies were performed on the right side above the target coordinates and the dura mater was incised immediately before electrode implantation. Custom-made tungsten electrodes[67] were targeted at DH (CA1; 3.0 mm posterior and 1.5 mm lateral to bregma, 3.0 mm ventral to the brain surface), VH (CA1; 5.0 mm posterior and 4.8 mm lateral to bregma, 6.3 mm ventral to the brain surface), PL (2.5 mm anterior and 0.5–0.8 mm lateral to bregma, 3.0 mm ventral to the brain surface), and BLA (basal nucleus; 2.8 mm posterior and 4.7 mm lateral to bregma, 7.2 mm ventral to the brain surface)[68]. The electrodes were loaded into a microdrive (VersaDrive-8, Neuralynx, MT) and the implant was secured to the anchoring screws with light-cured dental cement (Henry Schein, UK). Another analgesic (meloxicam, 1 mg/kg, s.c.) was given at the end of surgery. Rats were singly housed for 1–2 days after surgery, after which they were group housed as above. Buprenorphine and meloxicam were given once daily for 2–3 days after surgery. Behavioral testing commenced 6–8 days after surgery.

Drug injection

SCH23390 hydrochloride (0.1 mg/kg, i.p.; Tocris Bioscience, UK) was dissolved in 0.9% sterile saline (1 mL/kg) and injected 30 min before CFC (see below). We have previously shown that this dose impairs CFC[23,24]. Vehicle-treated controls received injections of 0.9% sterile saline (1 mL/kg, i.p.). Animals were randomly assigned to receive SCH23390 or vehicle treatment.

Behavioral testing

The effects of systemic SCH23390 administration on CFC were investigated using a two-day conditioning and retrieval paradigm. Each rat was randomly allocated to receive SCH23390 or vehicle treatment before CFC. The

apparatus[69] and experimental procedures[24] used have been described in detail elsewhere. On the first day rats underwent conditioning in a novel context that consisted of distinct visual, auditory, and olfactory cues present in the background during CFC. The US was a mild electric shock delivered through the chamber floor bars automatically via a PC running Med-PC IV software (Med Associates, VT). The rat was placed in the chamber and after 2 min was presented with four shocks (0.5 mA, 0.5 s, 1 min inter-trial interval). The rat was removed from the chamber 2 min after presentation of the last shock and returned to the home cage. On the second day the rat was returned to the same conditioning chamber for 5 min to test memory retrieval drug-free. The floor bars and waste tray were cleaned with 40% ethanol between each session. Rats were tested at approximately the same time of day on both days. Electrophysiological recordings (see below) were obtained during CFC and retrieval testing. Behavior during retrieval testing was recorded using a digital camera (ViewPoint, France) positioned above the chamber.

Electrophysiological recordings

LFPs from the electrodes targeting each area were recorded during CFC and retrieval testing by connecting the microdrive via a headstage, cable, and pre-amplifier to an OmniPlex neural recording data acquisition system (Plexon Inc, TX). LFPs were band-pass filtered at 0.7–170 Hz and digitized at 1.25 kHz. A cable connecting the Med Associates and OmniPlex systems was used to record the start of the CFC and retrieval sessions, triggered by the Med-PC IV software, in the LFP data recording file.

Histology

After completing retrieval testing, rats were deeply anesthetized with sodium pentobarbital and current was passed through each electrode using an electrical stimulator to create a small lesion at the electrode tips. Rats were then perfused transcardially with 0.9% saline followed by 4% paraformaldehyde. The brains were removed, post-fixed in 4% paraformaldehyde, and kept at 4 °C until slicing. Sections containing the relevant areas were obtained using a vibratome and stained for acetylcholinesterase (Fig. 1D). Only data from rats with histologically confirmed electrode placements in DH, VH, PL, and/or BLA were included in the electrophysiological data analysis.

Behavioral data analysis

Freezing, defined as the absence of movement except in relation to respiration, was taken as the behavioral measure of contextual fear during retrieval testing. Freezing was quantified automatically using VideoTrack software (ViewPoint, France) by setting the freezing detection threshold to 100 pixels change/frame (25 frames/sec), based on a comparison between automatically determined and manually scored freezing levels from our published data[24]. The cumulative duration of freezing during retrieval testing was calculated and expressed as a percentage of the 5 min test duration. Differences in freezing between the two groups were analyzed in two ways. Average freezing over the whole 5 min test session was analyzed using a two-tailed unpaired t-test, with the data presented in a bar graph as the mean + standard error of the mean (SEM). Freezing during each 1-min bin was also analyzed separately using two-way analysis of variance (ANOVA) with repeated measures, with treatment as the between-subjects factor and time as the within-subjects factor. Freezing during each 1-min bin was presented in a line graph as the mean + SEM. The level of significance for both analyses was set at $P < 0.05$.

Electrophysiological data analysis

LFP activity was analyzed using multi-taper spectral analysis as described elsewhere[70–72]. LFP recordings were inspected visually and data containing obvious electrical noise artefacts were omitted from the analysis. LFP signals were normalized to unit variance in each segment prior to spectral analysis. Normalization removes effects of changes in absolute power due to changes in electrode impedance, therefore we report on differences in relative power. Spectral estimates for LFP data from each area in the 2 min period before US presentations during CFC and in the 5 min retrieval test were generated using custom Matlab scripts. LFP recordings from all areas contained many electrical noise artefacts in the 2 min period after US presentations during CFC, which precluded analysis of the data from this period.

We first examined the acute effects of SCH23390 on theta (4–12 Hz), low gamma (30–45 Hz), and high gamma (55–80 Hz) power in each area during CFC. The gamma frequency band was divided into low and high frequencies to omit electrical mains noise ~ 50 Hz. Differences between SCH23390 and vehicle treatment in power at each individual frequency throughout the theta and gamma bands were quantified using the log ratio test. The acute effects of SCH23390 on theta, low gamma, and high gamma coherence between the areas sharing direct anatomical connections (i.e. DH–VH, VH–PL, VH–BLA, and PL–BLA) were then determined during CFC as measures of synchrony between these areas. Differences between SCH23390 and vehicle treatment in coherence at each individual frequency throughout the theta and gamma bands were quantified using the chi-squared difference of coherence test. Power and coherence data are presented as the mean +/− 95% pointwise confidence intervals. The level of significance for the statistical comparisons of power and coherence was set at $P < 0.001$ to correct for multiple comparisons across individual frequencies. Differences at individual frequencies were also considered as chance effects, therefore differences were only deemed significant where they were found for two or more adjacent frequencies.

The acute effects of SCH23390 on theta-gamma PAC during CFC were quantified as described elsewhere[73–75] using custom Matlab scripts. Theta-gamma PAC was determined using a modulation index from the normalised mean vector length. Estimates were constructed using analytic Morse wavelets, with significance determined using surrogate data[75–77]. Amplitude information in each trial was split into five blocks, which were randomly permuted to yield a surrogate dataset for amplitude. Phases were shuffled randomly between the different

frequency components[78]. Each shuffled phase information obtained from the *i*th frequency was randomly matched with the shuffled amplitude data from the *j*th frequency, with *i* and *j* random integers. We examined theta-gamma PAC within each area and between the directly inter-connected areas. Specifically, we examined DH theta-VH gamma PAC since theta oscillations propagate from DH to VH[79,80]. We also examined VH theta-PL gamma PAC since hippocampal–prefrontal theta synchrony is mediated by VH[81,82]. Similarly, we examined VH theta-BLA gamma PAC since theta burst stimulation of VH modulates BLA activity and plasticity[83]. Finally, we examined PL theta-BLA gamma PAC since learned fear inhibition is associated with prefrontal theta coupling of BLA gamma[29]. Color plots of theta-gamma PAC within each area and between the directly inter-connected areas showed that peak theta phase coupling of gamma amplitude occurred at a theta frequency ~ 5 Hz after vehicle or SCH23390 treatment, therefore we focused the analyses at this theta frequency. Theta-gamma PAC was analyzed using two-way ANOVA with repeated measures, with treatment as the between-subjects factor and gamma frequency band as the within-subjects factor. Post-hoc comparisons were conducted using the Sidak test where indicated. Theta-gamma PAC was presented in bar graphs as the mean + SEM and the level of significance for the analyses was set at $P < 0.05$.

The effects of SCH23390 given before CFC on theta power and coherence, low and high gamma power and coherence, and theta-gamma PAC during retrieval testing drug-free were determined as above. We also examined differences in these neurophysiological measures between epochs of movement and freezing during retrieval testing in the vehicle-treated controls to determine if decreased freezing resulting from SCH23390 treatment before CFC was related specifically to impaired contextual fear or non-specifically to increased movement at retrieval. Freezing epochs were determined by considering intervals of a minimum of 0.5 s where < 100 pixels change/frame (i.e. the freezing detection threshold) was detected, while movement epochs were determined by considering intervals of a minimum of 0.5 s where > 500 pixels change/frame was detected. The resulting LFP data from these intervals were then pooled within and between rats. Differences between movement and freezing in theta power and coherence, low and high gamma power and coherence, and theta-gamma PAC during retrieval testing were determined as above.

Data availability

All electrophysiology data and analysis code are freely available online (https://osf.io/km2s7/).

Received: 25 June 2023; Accepted: 12 October 2023
Published online: 17 October 2023

References

1. Rudy, J. W., Huff, N. C. & Matus-Amat, P. Understanding contextual fear conditioning: Insights from a two-process model. *Neurosci. Biobehav. Rev.* **28**, 675–685 (2004).
2. Maren, S., Phan, K. L. & Liberzon, I. The contextual brain: Implications for fear conditioning, extinction and psychopathology. *Nat. Rev. Neurosci.* **14**, 417–428 (2013).
3. Chaaya, N., Battle, A. R. & Johnson, L. R. An update on contextual fear memory mechanisms: Transition between amygdala and hippocampus. *Neurosci. Biobehav. Rev.* **92**, 43–54 (2018).
4. Fanselow, M. S. From contextual fear to a dynamic view of memory systems. *Trends. Cogn. Sci.* **14**, 7–15 (2010).
5. Ohkawa, N. *et al.* Artificial association of pre-stored information to generate a qualitatively new memory. *Cell Rep.* **11**, 261–269 (2015).
6. Chang, S. D., Chen, D. Y. & Liang, K. C. Infusion of lidocaine into the dorsal hippocampus before or after the shock training phase impaired conditioned freezing in a two-phase training task of contextual fear conditioning. *Neurobiol. Learn. Mem.* **89**, 95–105 (2008).
7. Zelikowsky, M., Hersman, S., Chawla, M. K., Barnes, C. A. & Fanselow, M. S. Neuronal ensembles in amygdala, hippocampus, and prefrontal cortex track differential components of contextual fear. *J. Neurosci.* **34**, 8462–8466 (2014).
8. Kitamura, T. *et al.* Engrams and circuits crucial for systems consolidation of a memory. *Science* **356**, 73–78 (2017).
9. Shibano, N. *et al.* Excitation of prefrontal cortical neurons during conditioning enhances fear memory formation. *Sci. Rep.* **10**, 8613. https://doi.org/10.1038/s41598-020-65597-7 (2020).
10. Pitkänen, A., Pikkarainen, M., Nurminen, N. & Ylinen, A. Reciprocal connections between the amygdala and the hippocampal formation, perirhinal cortex, and postrhinal cortex in rat. A review. *Ann. N. Y. Acad. Sci.* **911**, 369–391 (2000).
11. Cenquizca, L. A. & Swanson, L. W. Spatial organization of direct hippocampal field CA1 axonal projections to the rest of the cerebral cortex. *Brain Res. Rev.* **56**, 1–26 (2007).
12. Huff, M. L., Emmons, E. B., Narayanan, N. S. & LaLumiere, R. T. Basolateral amygdala projections to ventral hippocampus modulate the consolidation of footshock, but not contextual, learning in rats. *Learn. Mem.* **23**, 51–60 (2016).
13. Kim, W. B. & Cho, J.-H. Synaptic targeting of double-projecting ventral CA1 hippocampal neurons to the medial prefrontal cortex and basal amygdala. *J. Neurosci.* **37**, 4868–4882 (2017).
14. Kim, W. B. & Cho, J. H. Encoding of contextual fear memory in hippocampal-amygdala circuit. *Nat. Commun.* **11**, 1382. https://doi.org/10.1038/s41467-020-15121-2 (2020).
15. Jimenez, J. C. *et al.* Contextual fear memory retrieval by correlated ensembles of ventral CA1 neurons. *Nat. Commun.* **11**, 3492. https://doi.org/10.1038/s41467-020-17270-w (2020).
16. Twining, R. C., Lepak, K., Kirry, A. J. & Gilmartin, M. R. Ventral hippocampal input to the prelimbic cortex dissociates the context from the cue association in trace fear memory. *J. Neurosci.* **40**, 3217–3230 (2020).
17. Likhtik, E. & Johansen, J. P. Neuromodulation in circuits of aversive emotional learning. *Nat. Neurosci.* **22**, 1586–1597 (2019).
18. Stubbendorff, C. & Stevenson, C. W. Dopamine regulation of contextual fear and associated neural circuit function. *Eur. J. Neurosci.* **54**, 6933–6947 (2021).
19. Oades, R. D. & Halliday, G. M. Ventral tegmental (A10) system: Neurobiology. 1. Anatomy and connectivity. *Brain Res.* **434**, 117–165 (1987).
20. Gasbarri, A., Sulli, A. & Packard, M. G. The dopaminergic mesencephalic projections to the hippocampal formation in the rat. *Prog. Neuropsychopharmacol. Biol. Psychiatry* **21**, 1–22 (1997).
21. Missale, C., Nash, S. R., Robinson, S. W., Jaber, M. & Caron, M. G. Dopamine receptors: From structure to function. *Physiol. Rev.* **78**, 189–225 (1998).
22. Inoue, T., Izumi, T., Maki, Y., Muraki, I. & Koyama, T. Effect of the dopamine D(1/5) antagonist SCH 23390 on the acquisition of conditioned fear. *Pharmacol. Biochem. Behav.* **66**, 573–578 (2000).

23. Heath, F. C. *et al.* Dopamine D1-like receptor signalling in the hippocampus and amygdala modulates the acquisition of contextual fear conditioning. *Psychopharmacology (Berl.)* **232**, 2619–2629 (2015).
24. Stubbendorff, C., Hale, E., Bast, T., Cassaday, H. J. & Stevenson, C. W. Dopamine D1-like receptors in the dorsomedial prefrontal cortex regulate contextual fear conditioning. *Psychopharmacology (Berl.)* **236**, 1771–1782 (2019).
25. Huang, Y. Y. & Kandel, E. R. D1/D5 receptor agonists induce a protein synthesis-dependent late potentiation in the CA1 region of the hippocampus. *Proc. Natl. Acad. Sci. U. S. A.* **92**, 2446–2450 (1995).
26. Gurden, H., Takita, M. & Jay, T. M. Essential role of D1 but not D2 receptors in the NMDA receptor-dependent long-term potentiation at hippocampal-prefrontal cortex synapses in vivo. *J. Neurosci.* **20**, RC106 (2000).
27. Li, C., Dabrowska, J., Hazra, R. & Rainnie, D. G. Synergistic activation of dopamine D1 and TrkB receptors mediate gain control of synaptic plasticity in the basolateral amygdala. *PLoS One* **6**, e26065. https://doi.org/10.1371/journal.pone.0026065 (2011).
28. Headley, D. B. & Paré, D. In sync: Gamma oscillations and emotional memory. *Front. Behav. Neurosci.* **7**, 170. https://doi.org/10.3389/fnbeh.2013.00170 (2013).
29. Stujenske, J. M., Likhtik, E., Topiwala, M. A. & Gordon, J. A. Fear and safety engage competing patterns of theta-gamma coupling in the basolateral amygdala. *Neuron* **83**, 919–933 (2014).
30. Bocchio, M., Nabavi, S. & Capogna, M. Synaptic plasticity, engrams, and network oscillations in amygdala circuits for storage and retrieval of emotional memories. *Neuron* **94**, 731–743 (2017).
31. Makino, Y., Polygalov, D., Bolaños, F., Benucci, A. & McHugh, T. J. Physiological signature of memory age in the prefrontal–hippocampal circuit. *Cell Rep.* **29**, 3835-3846.e5 (2019).
32. Totty, M. S. & Maren, S. Neural oscillations in aversively motivated behavior. *Front. Behav. Neurosci.* **16**, 936036. https://doi.org/10.3389/fnbeh.2022.936036 (2022).
33. Radiske, A. *et al.* Cross-frequency phase-amplitude coupling between hippocampal theta and gamma oscillations during recall destabilizes memory and renders it susceptible to reconsolidation disruption. *J. Neurosci.* **40**, 6398–6408 (2020).
34. Bo, P. & Savoldi, F. Comparative study of the EEG profile of neuroleptics selective for D-1 or D-2 dopamine receptors in the rabbit. *Pharmacol. Res.* **26**, 67–74 (1992).
35. Weiss, T., Veh, R. W. & Heinemann, U. Dopamine depresses cholinergic oscillatory network activity in rat hippocampus. *Eur. J. Neurosci.* **18**, 2573–2580 (2003).
36. Xu, X., Zheng, C., An, L., Wang, R. & Zhang, T. Effects of dopamine and serotonin systems on modulating neural oscillations in hippocampus-prefrontal cortex pathway in rats. *Brain. Topogr.* **29**, 539–551 (2016).
37. Park, A. J. *et al.* Reset of hippocampal-prefrontal circuitry facilitates learning. *Nature* **591**, 615–619 (2021).
38. Gonzalez, M. C. *et al.* Reactivation-dependent amnesia for object recognition memory is contingent on hippocampal theta-gamma coupling during recall. *Learn. Mem.* **29**, 1–6 (2021).
39. Parker, K. L., Chen, K. H., Kingyon, J. R., Cavanagh, J. F. & Narayanan, N. S. D1-dependent 4 Hz oscillations and ramping activity in rodent medial frontal cortex during interval timing. *J. Neurosci.* **34**, 16774–16783 (2014).
40. Ott, T., Westendorff, S. & Nieder, A. Dopamine receptors influence internally generated oscillations during rule processing in primate prefrontal cortex. *J. Cogn. Neurosci.* **30**, 770–784 (2018).
41. Lorétan, K., Bissière, S. & Lüthi, A. Dopaminergic modulation of spontaneous inhibitory network activity in the lateral amygdala. *Neuropharmacology* **47**, 631–639 (2004).
42. Dejean, C. *et al.* Prefrontal neuronal assemblies temporally control fear behaviour. *Nature* **535**, 420–424 (2016).
43. Karalis, N. *et al.* 4-Hz oscillations synchronize prefrontal–amygdala circuits during fear behavior. *Nat. Neurosci.* **19**, 605–612 (2016).
44. Ozawa, M. *et al.* Experience-dependent resonance in amygdalo-cortical circuits supports fear memory retrieval following extinction. *Nat. Commun.* **11**, 4358. https://doi.org/10.1038/s41467-020-18199-w (2020).
45. Amir, A., Headley, D. B., Lee, S. C., Haufler, D. & Paré, D. Vigilance-associated gamma oscillations coordinate the ensemble activity of basolateral amygdala neurons. *Neuron* **97**, 656-669.e7 (2018).
46. Foo, S. & Bohbot, V. D. Theta rhythm across the species: Bridging inconsistencies with a multiple memory systems approach. *Behav. Neurosci.* **134**, 475–490 (2020).
47. Nuñez, A. & Buño, W. The theta rhythm of the hippocampus: From neuronal and circuit mechanisms to behavior. *Front. Cell Neurosci.* **15**, 649262. https://doi.org/10.3389/fncel.2021.649262 (2021).
48. Bourne, J. A. SCH 23390: the first selective dopamine D1-like receptor antagonist. *CNS Drug Rev.* **7**, 399–414 (2001).
49. Miller, A. M. P., Frick, B. J., Smith, D. M., Radulovic, J. & Corcoran, K. A. Network oscillatory activity driven by context memory processing is differently regulated by glutamatergic and cholinergic neurotransmission. *Neurobiol. Learn. Mem.* **145**, 59–66 (2017).
50. Seidenbecher, T., Laxmi, T. R., Stork, O. & Pape, H. C. Amygdalar and hippocampal theta rhythm synchronization during fear memory retrieval. *Science* **301**, 846–850 (2003).
51. Pape, H. C., Narayanan, R. T., Smid, J., Stork, O. & Seidenbecher, T. Theta activity in neurons and networks of the amygdala related to long-term fear memory. *Hippocampus* **15**, 874–880 (2005).
52. Albrecht, A., Bergado-Acosta, J. R., Pape, H. C. & Stork, O. Role of the neural cell adhesion molecule (NCAM) in amygdalo-hippocampal interactions and salience determination of contextual fear memory. *Int. J. Neuropsychopharmacol.* **13**, 661–674 (2010).
53. Lesting, J. *et al.* Directional theta coherence in prefrontal cortical to amygdalo–hippocampal pathways signals fear extinction. *PLoS ONE* **8**, e77707. https://doi.org/10.1371/journal.pone.0077707 (2013).
54. Lesting, J. *et al.* Patterns of coupled theta activity in amygdala-hippocampal-prefrontal cortical circuits during fear extinction. *PLoS ONE* **6**, e21714. https://doi.org/10.1371/journal.pone.0021714 (2011).
55. Bauer, E. P., Paz, R. & Paré, D. Gamma oscillations coordinate amygdalo-rhinal interactions during learning. *J. Neurosci.* **27**, 9369–9379 (2007).
56. Popescu, A. T., Popa, D. & Paré, D. Coherent gamma oscillations couple the amygdala and striatum during learning. *Nat. Neurosci.* **12**, 801–807 (2009).
57. Kanta, V., Paré, D. & Headley, D. B. Closed-loop control of gamma oscillations in the amygdala demonstrates their role in spatial memory consolidation. *Nat. Commun.* **10**, 3970. https://doi.org/10.1038/s41467-019-11938-8 (2019).
58. Tang, W., Kochubey, O., Kintscher, M. & Schneggenburger, R. A. VTA to basal amygdala dopamine projection contributes to signal salient somatosensory events during fear learning. *J. Neurosci.* **40**, 3969–3980 (2020).
59. Maren, S. & Fanselow, M. S. Synaptic plasticity in the basolateral amygdala induced by hippocampal formation stimulation in vivo. *J. Neurosci.* **15**, 7548–7564 (1995).
60. Dolleman-van der Weel, M. J. *et al.* The nucleus reuniens of the thalamus sits at the nexus of a hippocampus and medial prefrontal cortex circuit enabling memory and behavior. *Learn. Mem.* **26**, 191–205 (2019).
61. Ramanathan, K. R., Jin, J., Giustino, T. F., Payne, M. R. & Maren, S. Prefrontal projections to the thalamic nucleus reuniens mediate fear extinction. *Nat. Commun.* **9**, 4527. https://doi.org/10.1038/s41467-018-06970-z (2018).
62. Silva, B. A. *et al.* A thalamo-amygdalar circuit underlying the extinction of remote fear memories. *Nat. Neurosci.* **24**, 964–974 (2021).
63. Xu, W. & Südhof, T. C. A neural circuit for memory specificity and generalization. *Science* **339**, 1290–1295 (2013).
64. Venkataraman, A. *et al.* Incerto-thalamic modulation of fear via GABA and dopamine. *Neuropsychopharmacology* **46**, 1658–1668 (2018).

65. Thörn, C. W., Kafetzopoulos, V. & Kocsis, B. Differential effect of dopamine D4 receptor activation on low-frequency oscillations in the prefrontal cortex and hippocampus may bias the bidirectional prefrontal–hippocampal coupling. *Int. J. Mol. Sci.* **23**, 11705. https://doi.org/10.3390/ijms231911705 (2022).
66. Percie du Sert, N. *et al.* Reporting animal research: Explanation and elaboration for the ARRIVE guidelines 2.0. *PLoS Biol.* **18**, e3000411. https://doi.org/10.1371/journal.pbio.3000411 (2020).
67. Stubbendorff, C., Molano-Mazon, M., Young, A. M. J. & Gerdjikov, T. V. Synchronization in the prefrontal–striatal circuit tracks behavioural choice in a go-no-go task in rats. *Eur. J. Neurosci.* **49**, 701–711 (2019).
68. Paxinos, G. & Watson, C. *The Rat Brain in Stereotaxic Coordinates* 6th edn. (Academic Press, 2007).
69. Stevenson, C. W., Spicer, C. H., Mason, R. & Marsden, C. A. Early life programming of fear conditioning and extinction in adult males. *Behav. Brain Res.* **205**, 505–510 (2009).
70. Fenton, G. E., Halliday, D. M., Mason, R. & Stevenson, C. W. Medial prefrontal cortex circuit function during retrieval and extinction of associative learning under anesthesia. *Neuroscience* **265**, 204–216 (2014).
71. Fenton, G. E., Spicer, C. H., Halliday, D. M., Mason, R. & Stevenson, C. W. Basolateral amygdala activity during the retrieval of associative learning under anesthesia. *Neuroscience* **233**, 146–156 (2013).
72. Day, H. L. L., Suwansawang, S., Halliday, D. M. & Stevenson, C. W. Sex differences in auditory fear discrimination are associated with altered medial prefrontal cortex function. *Sci. Rep.* **10**, 6300. https://doi.org/10.1038/s41598-020-63405-w (2020).
73. Canolty, R. T. *et al.* High gamma power is phase-locked to theta oscillations in human neocortex. *Science* **313**, 1626–1628 (2006).
74. Samiee, S. & Baillet, S. Time-resolved phase-amplitude coupling in neural oscillations. *Neuroimage* **159**, 270–279 (2017).
75. Suwansawang, S. & Halliday, D. M. Time-frequency based coherence and phase locking value analysis of human locomotion data using generalized Morse wavelets. In *Proceedings of the 10th International Joint Conference on Biomedical Engineering Systems and Technologies (BIOSTEC 2017)*, 34–41. https://doi.org/10.5220/0006111800340041 (2017).
76. Lilly, J. M. & Olhede, S. C. Generalized Morse wavelets as a superfamily of analytic wavelets. *IEEE Trans. Signal Process.* **60**, 6036–6041 (2012).
77. Aru, J. *et al.* Untangling cross-frequency coupling in neuroscience. *Curr. Opin. Neurobiol.* **31**, 51–61 (2015).
78. Thengone, D., Gagnidze, K., Pfaff, D. & Proekt, A. Phase-amplitude coupling in spontaneous mouse behavior. *PLoS One* **11**, e0162262. https://doi.org/10.1371/journal.pone.0162262 (2016).
79. Lubenov, E. V. & Siapas, A. G. Hippocampal theta oscillations are travelling waves. *Nature* **459**, 534–539 (2009).
80. Patel, J., Fujisawa, S., Berényi, A., Royer, S. & Buzsáki, G. Traveling theta waves along the entire septotemporal axis of the hippocampus. *Neuron* **75**, 410–417 (2012).
81. Adhikari, A., Topiwala, M. A. & Gordon, J. A. Synchronized activity between the ventral hippocampus and the medial prefrontal cortex during anxiety. *Neuron* **65**, 257–269 (2010).
82. O'Neill, P. K., Gordon, J. A. & Sigurdsson, T. Theta oscillations in the medial prefrontal cortex are modulated by spatial working memory and synchronize with the hippocampus through its ventral subregion. *J. Neurosci.* **33**, 14211–14224 (2013).
83. Bazelot, M. *et al.* Hippocampal theta input to the amygdala shapes feedforward inhibition to gate heterosynaptic plasticity. *Neuron* **87**, 1290–1303 (2015).

Acknowledgements

This work was funded by a research grant from the Biotechnology and Biological Sciences Research Council [Grant Number BB/P001149/1].

Author contributions

C.S. and E.H. conducted the experiments. C.S., S.S., and D.M.H. analyzed the data. T.B., H.J.C., S.J.M., and C.W.S. conceived the study and designed the experiments. C.S. and C.W.S. drafted the manuscript. C.S., T.B., H.J.C., S.J.M., D.M.H., and C.W.S. revised the manuscript.

Competing interests

The authors declare no competing interests.

Additional information

Supplementary Information The online version contains supplementary material available at https://doi.org/10.1038/s41598-023-44772-6.

Correspondence and requests for materials should be addressed to C.S. or C.W.S.